Available online at www.sciencedirect.com
SCIENCE DIRECT®
Journal of Power Sources 115 (2003) 81–89
JOURNAL OF POWER SOURCES
www.elsevier.com/locate/jpowsour

Single domain PEMFC model based on agglomerate catalyst geometry

N.P. Siegel, M.W. Ellis*, D.J. Nelson, M.R. von Spakovsky

Department of Mechanical Engineering, Virginia Polytechnic and State University, Blacksburg, VA, USA

Received 7 November 2002; accepted 17 November 2002

Abstract

A steady two-dimensional computational model for a proton exchange membrane (PEM) fuel cell is presented. The model accounts for species transport, electrochemical kinetics, energy transport, current distribution, and water uptake and release in the catalyst layer. The governing differential equations are solved over a single computational domain, which consists of a gas channel, gas diffusion layer, and catalyst layer for both the anode and cathode sides of the cell as well as the solid polymer membrane. The model for the catalyst regions is based on an agglomerate geometry, which requires water species to exist in both dissolved and gaseous forms simultaneously. Data related to catalyst morphology, which was required by the model, was obtained via a microscopic analysis of a commercially available membrane electrode assembly (MEA). The coupled set of differential equations is solved with the commercial computational fluid dynamics (CFD) solver, CFDesign™, and is readily adaptable with respect to geometry and material property definitions. The results show that fuel cell performance is highly dependent on catalyst structure, specifically the relative volume fractions of gas pores and polymer membrane contained within the active region as well as the geometry of the individual agglomerates.

Keywords: PEM fuel cell; Modeling; Catalyst layer; Agglomerate

1. Introduction

In recent years, the proton exchange membrane (PEM) fuel cell has received a great deal of attention, from the automotive industry in particular, as a candidate for near-future power generation applications. PEM fuel cells are particularly suited to automotive applications primarily because of their relatively low operating temperature, efficiency, and high power density that is comparable to existing internal combustion technology. However, like many emerging technologies, PEM fuel cells must overcome certain engineering and economic obstacles if they are ever to become commercially viable. In short, PEM fuel cells must become more efficient and lower in cost. Improvements in cell design and materials development can help to achieve these goals. There are two approaches to improving cell design and materials development. The first is to design and build test cells and evaluate their performance. This method can yield useful information, but it is also costly and time consuming. In addition, although it is relatively easy to evaluate a cell's total current and voltage and from these generate a polarization curve, it is much more difficult to evaluate operating parameters in situ, which is vital to understanding how a design performs over a range of operating conditions. In order to obtain data such as reactant concentration profiles, membrane hydration, and temperature distributions inside the cell, it is more convenient to simulate the fuel cell with a mathematical model.

In the past, most mathematical models focused on the cathode side of the fuel cell only; the reason being that the cathode activation overpotential is the single largest source of inefficiency in the fuel cell. These models also typically include the membrane, as it contributes to ohmic overpotential, and the gas diffusers. The catalyst layer itself has generally been modeled as an interface and denoted the point at which source terms for species consumption or production were applied. The work by Springer et al. [1] laid the foundation for many future numerical models. In their paper, they present a one-dimensional model, the principal focus of which is water transport through the membrane. Their model shows that the net water transport per proton is much less than the measured electro-osmotic drag coefficient for a fully hydrated membrane, which indicates the presence of other important water transport mechanisms. Bernardi and Verbrugge [2] present a model with the focus on species transport, electrochemistry, and catalyst utilization in which they conclude, among other things, that the transport of gases

* Corresponding author. Tel.: +1-540-231-9102.
E-mail address: mwellis@vt.edu (M.W. Ellis).

0378-7753/02/$ – see front matter
PII: S0378-7753(02)00622-5

dissolved in the polymer phase of the electrodes affects catalyst utilization and limits cell performance. This model is based on a pseudo-homogeneous catalyst layer structure in which the layer has no pores through which gas can be transported to the reaction sites. Rather, the reactants must dissolve into the polymer phase and diffuse through the non-porous catalyst layer to reach the reaction sites. This approach can be computationally advantageous as the equations describing transport in the catalyst layer are relatively simple. The disadvantage is that the pseudo-homogenous catalyst layer structure does not allow for transport of reactants in the gas phase within this layer. Research has shown that the catalyst layer is porous and that reactants can be transported throughout in the gas phase [3,4]. The model of Broka and Ekdunge [4] represents one of the first applications of an agglomerate catalyst layer structure to a PEM model. In this model, Broka and Ekdunge show, through microscopic analysis, that the catalyst layer is made up of clumps of carbon-supported Pt catalyst surrounded by a thin layer of Nafion and separated by pores. These clumps are referred to as agglomerates. The principal difference between this type of model and the pseudo-homogenous model is that in the agglomerate model, reactants can move in the gas phase rather than solely as a dissolved species through the catalyst layer. Broka and Ekdunge also show that the agglomerate model is better suited to modeling fuel cell behavior at high current densities, where concentration overpotential becomes dominant. In their model, they assume that the gaseous reactant concentration is constant across the catalyst layer. In the model presented in this paper, the reactant concentration is treated as variable.

In recent years, modeling efforts, both our own [5–7] and that of others (e.g. [8–12]), have increased in complexity. Most current models are multi-dimensional, include mass transport of multiple species, and include the entire fuel cell geometry from one gas channel to the other. Some models also account for two-phase flow, which is necessary when modeling the effects of liquid water production and flooding. Zhou and Liu [8] developed a three-dimensional fuel cell model based on the earlier work of Gurau et al. [9]. As part of the work they show how the model solution is affected when transitioning from a two-dimensional to a three-dimensional geometry. Their model focuses on species transport as well as current and temperature distribution. To solve the model, they partitioned the solution domain into three coupled regions, which is a more involved process for the user than is the single domain approach used in this work. In addition, water uptake and release within the polymer portion of the catalyst layers is neglected. Um et al. [10] present a transient, three-dimensional model and show that an interdigitated flow field can help to reduce mass transfer limitations. They use a single domain solution approach and neglect water uptake and release in the catalyst layer. Shimpalee et al. [11] also present a three-dimensional model but do not include transport through the catalyst layer as it is modeled as an interface. They show that the direction of water transport through the membrane can affect current density distribution patterns. A model including two-phase flow is presented by Natarajan et al. [12]. They show that liquid water buildup in the cathode has a substantial influence on cell performance. Their model is two-dimensional and focuses on liquid water transport in the porous media of the gas diffuser. The catalyst layer is an interface and only the cathode side of the cell is included. It should be noted that with the exception of Broka and Ekdunge, all of the models mentioned above either treat the catalyst layer as a pseudo-homogeneous film or simply as an interface.

This paper describes a mathematical model that simulates the transport of gaseous species, energy, protonic current, and water dissolved in the polymer phase of the catalyst layers and membrane. The catalyst layer is modeled as having an agglomerate structure, and the effect of catalyst layer structure on cell performance is also examined. The model is based on the finite element method and is formulated as a single solution domain problem. Consequently, interface conditions between the individual fuel cell elements need not be specified, and the only boundary conditions required are at the outer surfaces of the model.

2. Model development

Fig. 1 shows the solution domain of the model. In the anode and cathode gas channels, fuel and oxidant flow along the surface of the membrane electrode assembly. In these regions, the flow is considered to be laminar. Reactants move from the gas channels into the gas diffusion layers (GDL) which consist of a thin sheet of carbon paper, the purpose of

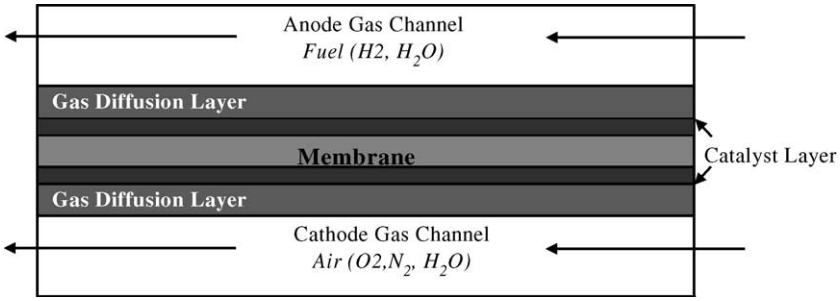

Fig. 1. Solution domain.

which is to evenly distribute the reactants across the catalyst layers and provide an electrical connection with the collector plate (not shown). The catalyst layers are among the more important parts of the fuel cell as it is within these regions where all of the electrochemical reactions take place. A large portion of the work presented in this model involves the characterization and modeling of the catalyst layers. The polymer membrane, which is assumed to be impermeable to reactant gases, transports only protons and dissolved water. Both ionic conductivity and ionomer content in the MEA have a significant of impact on cell performance.

2.1. Catalyst layer structure

To develop an accurate description of the catalyst layer, a 5 cm^2 MEA was purchased from ElectroChem Inc. Cross sections of the MEA were prepared and analyzed with a scanning electron microscope (SEM) and a transmission electron microscope (TEM). The cross sections for SEM analysis were prepared by three methods in order to evaluate which worked best. The first method involved freezing the sample in liquid nitrogen and fracturing it. This technique provided a clean section for viewing but also caused the gas diffusion layer to de-laminate from the assembly. The second method was to simply cut the MEA at room temperature with a razor. The blade was pushed directly down on top of the MEA as opposed to cutting across it. This also resulted in a clean section, but there was some dragging of the polymer through the sample as it is fairly malleable at room temperature. For the third method, the sample was frozen in liquid nitrogen and then cut as per the second method. This provided the best results of all.

Preparation of the cross sections for TEM analysis involved encasing the sample in epoxy and then using a diamond knife, or microtome, to slice off very thin sections (∼70 nm) for viewing. The samples were cut at room temperature.

The structure of the fuel cell MEA is shown in Fig. 2. The region labeled A in this image is the gas diffusion layer. Region B is the catalyst layer. In this region there is no carbon paper, only polymer encapsulated catalyst sites called agglomerates. Region C is the polymer membrane.

Fig. 3 shows a higher magnification view of the catalyst layer labeled B in Fig. 2. Fig. 3 along with Fig. 2 can be used to estimate the mean agglomerate size, the thickness of the active layer, and the void fraction of the active layer. The agglomerate size and void fraction were evaluated through the use of image analysis and enhancement software. By enhancing the SEM and TEM images, it is possible to highlight certain catalyst characteristics of interest and perform quantitative analyses. Geometric information about the catalyst structure can be used in conjunction with manufacturer's data for catalyst loading to estimate the specific catalyst area. Pores can be seen in the catalyst layer on the order of 1–10 μm in size. These are referred to as macropores.

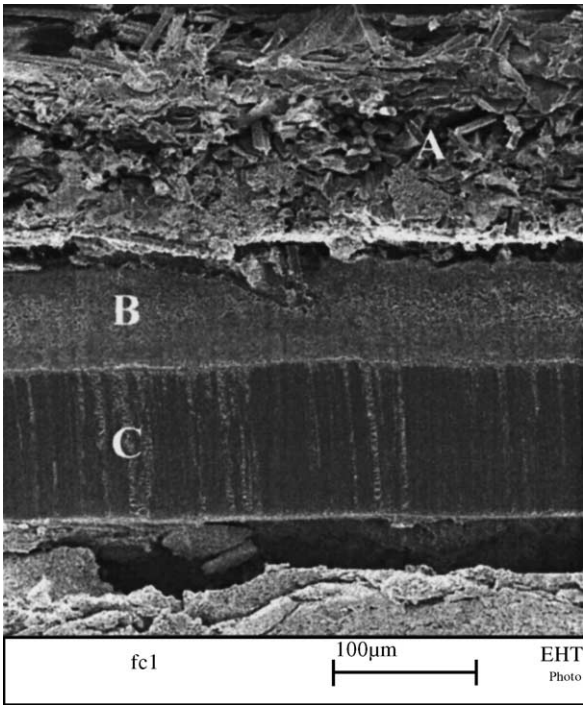

Fig. 2. Freeze cut cross section of ElectroChem MEA. Image magnification is 200×.

Fig. 4 shows a schematic of the agglomerate catalyst layer geometry used in this model. Reactant gas flows through the catalyst macro-pores and then dissolves into and diffuses through the agglomerate to the carbon-supported platinum reaction sites.

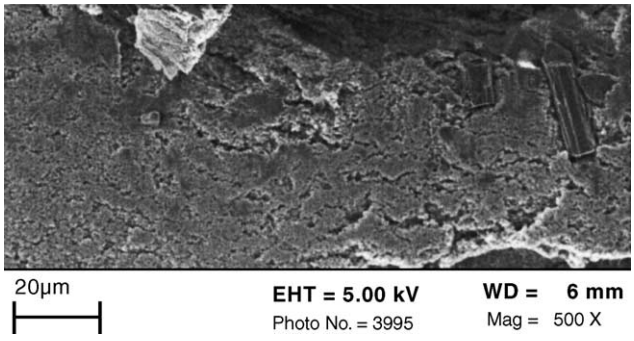

Fig. 3. Room temperature cut section of MEA showing the catalyst layer. Image magnification is 500×.

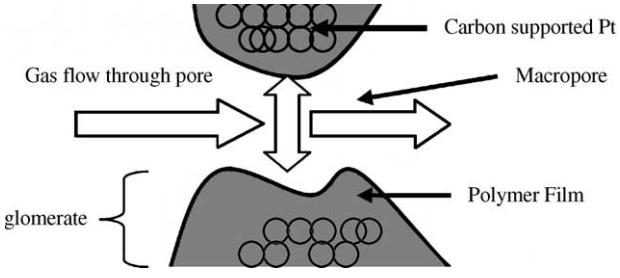

Fig. 4. Agglomerate catalyst geometry.

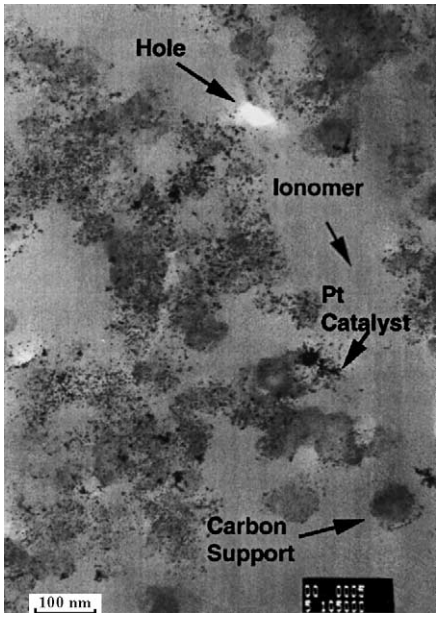

Fig. 5. TEM image of an agglomerate. Magnification is 18,400×.

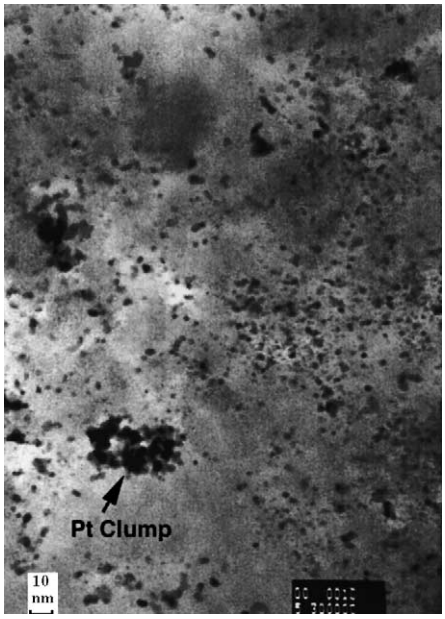

Fig. 6. TEM image of an agglomerate showing Pt catalyst particles and clumping. Image magnification is 485,500×.

Figs. 5 and 6 show TEM images of an agglomerate. In these images, it is possible to see the individual Pt catalyst particles as well as the carbon support. As indicated in Fig. 5, the light gray area between the carbon and Pt particles is ionomer. The white areas are holes, not to be confused with pores. These holes result from the pullout of carbon-supported catalyst during sample preparation. Indeed, nanoscale pores are absent from the TEM images. This is an important observation as it indicates that gas transfer in the porous catalyst is facilitated primarily by macro-pores on the order of 1–10 μm in size.

Fig. 6 is a higher magnification image in which the Pt catalyst particles are well defined. These Pt particles are nominally 3 nm in diameter. However, as a consequence of the technique used to deposit the catalyst, the individual particles have a tendency to clump together. When the catalyst particles form clumps, there is a reduction in the amount of surface area available for reaction, which can be viewed as a decrease in catalyst utilization.

The physical parameters used in the model can be found in Table 5. These parameters, some of which were determined by the microscopic analyses discussed earlier, must be used in conjunction with the appropriate mathematical relations to accurately model fuel cell performance.

2.2. Governing equations and closure relations

Eq. (1) in Table 1 reflects conservation of mass for all gas species. A source term reflects changes in the overall gas-phase mass due to consumption or production of gas species via reaction and mass transfer between the water in the gas phase and that dissolved in the polymer. The total density of the gas mixture is expressed as the sum of the individual species concentrations multiplied by their respective molar masses.

The momentum equations, Eqs. (2a) and (2b), are expressed as the Navier–Stokes equations in vector form, modified with a source term to account for Darcy flow in the

Table 1
Governing equations

Governing equation	Vector form of equation	Equation
Global continuity	$\nabla \cdot (\rho^g \bar{u}) = S_{H_2} + S_{O_2} + S_{vap} + S_{diss}$	1
Momentum	$\bar{u} \cdot \nabla[\rho^g u_x] = -\partial P/\partial x + \mu \nabla^2 u_x + S_{Darx}$	2a
	$\bar{u} \cdot \nabla[\rho^g u_y] = -\partial P/\partial y + \mu \nabla^2 u_y + S_{Dary}$	2b
Hydrogen transport	$\nabla \cdot (D_{H_2} \nabla c_{H_2}) - \bar{u} \nabla c_{H_2} + S_{H_2} = 0$	3
Water vapor transport	$\nabla \cdot (D_{vH_2O} \nabla c_{vH_2O}) - \bar{u} \nabla c_{vH_2O} + S_{vap} + S_{diss} = 0$	4
Oxygen transport	$\nabla \cdot (D_{O_2} \nabla c_{O_2}) - \bar{u} \nabla c_{O_2} + S_{O_2} = 0$	5
Nitrogen transport	$\nabla \cdot (D_{N_2} \nabla c_{N_2}) - \bar{u} \nabla c_{N_2} = 0$	6
Dissolved water transport	$\nabla \cdot (D_m \nabla c_m) + S_{drag} - S_{diss} = 0$	7
Potential membrane	$\nabla \cdot (\sigma_m \nabla \phi_m) = S_{em}$	8
Thermal energy	$\nabla \cdot [k^{eff} \nabla T] - \rho c_{eff} \bar{u} \nabla T + S_{om} + S_{rev} + S_{act} - S_{pl} - S_{pc} - S_{evap} = 0$	9

Table 2
Source terms

Source term	Equation	Application
Darcy flow in x-direction, $S_{\mathrm{Darx}} = C\mu u_x$	10	Anode and cathode: GDL, catalyst
Darcy flow in y-direction, $S_{\mathrm{Dary}} = C\mu u_y$	11	Anode and cathode; GDL, catalyst
Hydrogen consumption, $S_{\mathrm{H_2}} = -(1/2F)\,\mathrm{BV}$	12	Anode catalyst
Water vapor production, $S_{\mathrm{vap}} = (1/2F)\,\mathrm{BV}$	13	Cathode catalyst
Vapor/dissolved water mass transfer, $S_{\mathrm{diss}} = h_{\mathrm{mass}}(c_{\mathrm{m}}^{v} - c_{v\mathrm{H_2O}})$	14	Cathode catalyst
Oxygen consumption, $S_{\mathrm{O_2}} = -(1/4F)\,\mathrm{BV}$	15	Cathode catalyst
Electro-osmotic drag, $S_{\mathrm{drag}} = -(2.5/22F)\,(\partial\lambda/\partial x)\sigma(\partial\varphi/\partial x)$	16	Anode and cathode: catalyst, membrane
Protonic current, $S_{\mathrm{em}} = -\mathrm{BV}$	17	Anode and cathode: catalyst
Ohmic heating, $S_{\mathrm{om}} = (\sigma_{\mathrm{m}}\partial\phi_{\mathrm{m}}/\partial x)^2(1/\sigma_{\mathrm{m}})$	18	Anode and cathode: catalyst
Reversible heat, $S_{\mathrm{rev}} = T(\mathrm{BV}/F)\left[\sum_{p-r} s_{\mathrm{f}}^{\mathrm{o}}/n\right]$	19	Anode and cathode: catalyst
Activation loss, $S_{\mathrm{act}} = (\phi_{\mathrm{c}} - \phi_{\mathrm{m}})\,\mathrm{BV}$	20	Anode and cathode: catalyst
Water vaporization, $S_{\mathrm{pc}} = (\mathrm{BV}/2F)\,h_{\mathrm{fg}}$	21	Cathode catalyst
Vapor/dissolved phase change, $S_{\mathrm{evap}} = h_{\mathrm{fg}}S_{\mathrm{diss}}$	22	Anode and cathode: catalyst
Collector plate heat sink, $S_{\mathrm{pl}} - [(T - T_{\mathrm{pl}})/((t_{\mathrm{gdl}}/k_{\mathrm{gdl}}) + (t_{\mathrm{coll}}/k_{\mathrm{coll}}))]\,1/t_{\mathrm{gdl}}$	23	Anode and cathode; GDL

porous regions of the model. The Darcy source is active in the GDL and catalyst layers only; the inertial and viscous terms are neglected in these regions.

The gas species equations are given in Eqs. (3)–(6). The diffusion coefficients are based on a simplification of the Stefan–Maxwell equations and are modified by a porosity factor [9]. Each of these equations has an advective term equal to the product of velocity and concentration gradient. The general form of these equations would also include the complement to this term, the product of concentration and velocity gradient. In preliminary simulations, the velocity gradient was found to be negligible for most of the solution domain, with the exception of the inlet and exit, and for this reason the product of concentration and velocity gradient is omitted from the gas species equations. The source terms for hydrogen and oxygen species, Eqs. (12) and (15) in Table 2, account for consumption via reaction. The source term for water vapor accounts for production of water at the cathode, Eq. (13).

Water exists in dissolved form within the polymer membrane and a portion of the polymer phase of the catalyst layer. Dissolved water is transported through the polymer by diffusion and electro-osmotic drag only. A convective term would have to be added if the gas pressures in the anode and cathode were different; for this work the anode and cathode pressures are within 3% of each other and so the convective transport of water through the MEA is neglected. A source term is needed to account for mass transfer between the dissolved and vapor phases within the catalyst layer. This term, Eq. (14), is applied to both the dissolved water species equation and to the water vapor equation. Eq. (7) is the transport equation for dissolved water.

The transport of protons in the polymer portions of the fuel cell is described by Eq. (8). The source term, Eq. (17), represents the production/consumption of protons via the electrochemical reactions in the catalyst layers. The rate of the electrochemical reaction is described by the Butler–Volmer relation, Eq. (24). The electrical potential is assumed to be constant over each electrode. It is set to zero on the anode side and to the difference between the cell voltage and the open circuit voltage on the cathode side.

The energy equation is expressed by Eq. (9) and contains sources for ohmic heating due to ionic resistance Eq. (18), reversible heat Eq. (19), heat produced via activation losses Eq. (20), and heat exchange involved in the phase change of water. There are two terms related to phase change energy transfer. The first accounts for the energy needed to vaporize the water produced via reaction Eq. (21). One of the assumptions of this model is that water is produced in the liquid phase and instantly vaporized, provided that the cathode stream is not saturated. The energy required for the vaporization must then be included. The other term accounts for water moving between the dissolved and vapor phases Eq. (22). The enthalpy of the water dissolved in the polymer is assumed to be the same as the enthalpy of liquid water.

In this model, the collector plates are not included in the solution domain. In an actual fuel cell, the shoulder of the plates would be in contact with the MEA and provide a low-resistance pathway for heat. The source term S_{pl} Eq. (23) approximates the amount of heat that would move through the collector plates had they been part of the solution domain.

Table 3 contains the closure relations needed to complete the mathematical model. Eq. (24) is the Butler–Volmer equation as expressed for an agglomerate catalyst geometry [4]. The first term in the denominator effectively sets the maximum flux of reactant that can pass through the polymer layer surrounding an agglomerate. This term is based on a dissolved gas concentration at the gas/polymer interface given by a Henry's law relation, Eq. (26). The reactant flux limit establishes the limiting current of the cell. The second term in the denominator includes the reaction rate, Eq. (25), and is similar to that used by Broka and Ekdunge. with the exception that in this model the concentration of reactant (either oxygen or hydrogen) is assumed to vary across the

Table 3
Closure relations

Butler–Volmer, BV (A/nm^3)	$\mathrm{BV} = nF/((\delta/a)/C^*D_{\mathrm{m},k}) + 1/kE$	24
Reaction rate, k (mol/mm^3 s)	$k = A_{v1}i_{0,\mathrm{e}}/nF(c^*/c_{k,\mathrm{ref}})^{\gamma}[\mathrm{e}^{(\phi_\mathrm{c}-\phi_\mathrm{m})\alpha_\mathrm{a}F/RT} - \mathrm{e}^{-(\phi_\mathrm{c}-\phi_\mathrm{m})\alpha_\mathrm{c}F/RT}]$	25
Dissolved gas concentration, c^* (mol/mm^3)	$c^* = h_{\mathrm{d},\mathrm{e}}Tc_k$	26
Effectiveness, E	$E = \tanh(mL)/mL$	27
Thiele's modulus, mL	$mL = L\sqrt{k/(c^*D_{\mathrm{m,g}})}$	28
Gas species diffusion coefficient, D_k (mm^2/s)	$D_k = [((1 - c_kMW_k)/\rho)/\sum_{k\neq j}(c_j/c_{\mathrm{tol}}D_{jk})]\,\tau^{1.5}$	29
Diffusion coefficient for dissolved water, D_m (mm^2/s)	$D_\mathrm{m} = 1.3\mathrm{E}-4\,\mathrm{e}^{2416(1/303)-(1/T)}$	31
Protonic conductivity, σ_m $(\Omega\,\mathrm{mm})^{-1}$	$\sigma_\mathrm{m} = (0.005139\lambda - 0.000326)\,\mathrm{e}^{(1268/(1/303)-(1/T))}(\tau_\mathrm{g}\tau_\mathrm{m})$	32
Membrane water content, λ (mol H_2O/mol SO_3^-)	$\lambda = c_\mathrm{m}/((MW_\mathrm{m}/\rho_\mathrm{m}) - 0.0126\,c_\mathrm{m})$	34

width of the catalyst layer. Hence the term c^*, which is the dissolved reactant concentration, is not constant The effectiveness, given as Eq. (27), is a measure of how readily reactants diffuse through the agglomerates [4]. An effectiveness of 1.0 would indicate that reactants diffusing through the agglomerates encounter no resistance. Eq. (29) is an effective diffusion coefficient which allows for an approximate solution to the multi-component species equations without having to solve the full set of Stefan–Maxwell equations [9]. Eqs. (31) and (32) are the diffusion coefficients for water in Nafion and the ionic conductivity of Nafion, respectively [1]. Eq. (34) relates membrane water content to the dissolved water concentration while accounting for the swelling of the membrane with water sorption.

Table 4 contains a listing of the boundary conditions required by the model. Boundary conditions are specified at the inlets and outlets to both gas channels while the remaining external surfaces of the solution domain are assumed to have zero flux conditions.

Although the model presented does not include transient effects, initial conditions (ICs) are specified for the species equations as well as the dissolved water equation. Specifying ICs helps to stabilize the numerical solution and also decreases the amount of time needed to reach a converged solution. The ICs for the species equation are the same as the inlet boundary conditions. The dissolved water equation IC is set in a manner to be consistent with the water vapor equation to which it is coupled by Eq. (14).

In addition to the governing equations and closure relations, certain values for material properties and other physical parameters are needed to complete the model. The numerical values for the physical parameters used in the model are given in Table 5.

2.3. Numerical considerations

The outer surfaces of the gas channels shown in Fig. 1 are bounded by the collector plates (not shown) and are impermeable to gases. As part of the single domain formulation, each governing equation is solved throughout the entire domain, even if the equation is not physically valid in every region. This is accomplished using a variety of

Table 4
Boundary conditions for base case

Governing equation	Anode inlet	Anode exit	Cathode inlet	Cathode exit	Comments
Momentum	216 mm/s average velocity, parabolic profile	Fixed pressure	422 mm/s average velocity, parabolic profile	Fixed pressure	–
Hydrogen transport	$c_{\mathrm{H}_2} = 8.57\mathrm{E}-8$ mol/mm^3	$\nabla\cdot c_{\mathrm{H}_2} = 0$	$\nabla\cdot c_{\mathrm{H}_2} = 0$	$\nabla\cdot c_{\mathrm{H}_2} = 0$	Initial concentration in cathode is set to zero
Oxygen transport	$\nabla\cdot c_{\mathrm{O}_2} = 0$	$\nabla\cdot c_{\mathrm{O}_2} = 0$	$c_{\mathrm{O}_2} = 1.84\mathrm{E}-8$ mol/mm^3	$\nabla\cdot c_{\mathrm{O}_2} = 0$	Initial concentration in anode is set to zero.
Water vapor transport	$c_{v\mathrm{H}_2\mathrm{O}} = 8.65\mathrm{E}-9$ mol/mm^3	$\nabla\cdot c_{v\mathrm{H}_2\mathrm{O}} = 0$	$\nabla\cdot c_{v\mathrm{H}_2\mathrm{O}} = 7.98\mathrm{E}-9$ mol/mm^3	$\nabla\cdot c_{v\mathrm{H}_2\mathrm{O}} = 0$	–
Nitrogen transport	$\nabla\cdot c_{\mathrm{N}_2} = 0$	$\nabla\cdot c_{\mathrm{N}_2} = 0$	$c_{\mathrm{N}_2} = 6.94\mathrm{E}-8$ mol/mm^3	$\nabla\cdot c_{\mathrm{N}_2} = 0$	Initial concentration in anode is set to zero
Dissolved water transport	$\nabla\cdot c_\mathrm{m} = 0$	$\nabla\cdot c_\mathrm{m} = 0$	$\nabla\cdot c_\mathrm{m} = 0$	$\nabla\cdot c_\mathrm{m} = 0$	Initial concentration based on equilibrium with water vapor
Membrane potential	$\nabla\cdot\phi_\mathrm{m} = 0$	$\nabla\cdot\phi_\mathrm{m} = 0$	$\nabla\cdot\phi_\mathrm{m} = 0$	$\nabla\cdot\phi_\mathrm{m} = 0$	–
Energy	348.0 K	$\nabla\cdot T = 0$	348.0 K	$\nabla\cdot T = 0$	Constant temperature BC's along gas channels

Table 5
Physical parameters

Gas channel length, L_{gc} (cm)	6.6
Gas channel width, W (mm)	2.0
Gas channel height, H (mm)	2.0
Gas diffusion layer thickness, t_{gdl} (mm)	0.175
Catalyst layer thickness, t_{cat} (mm)	0.100
Membrane thickness, t_m (mm)	0.127
Collector thickness, t_{col} (mm)	3.0
Shoulder width, w (mm)	1.0
Reference temperature, T_{ref} (K)	298
Reference pressure, P_{ref} (atm)	1.0
Fixed charge concentration, c_{H+} (mol/m^3)	1,200.0
Gas diffusion layer void fraction, τ_g	0.5
Pt/carbon volume fraction in the catalyst layer, τ_{ptc}	0.19
Catalyst layer void fraction, τ_{cat}	0.09
Ionomer volume fraction in the catalyst layer, τ_{ion}	0.72
Air inlet relative humidity, Rh_c (%)	65
Fuel inlet relative humidity, Rh_a (%)	60
Faraday's constant, F (C/mol)	96,485
Permeability to air of gas diffusion layer, K (mm^{-2})	5.68×10^4
Cathode viscosity, μ_{air} (Pa s)	1.0×10^{-5}
Anode viscosity, μ_{H_2} (Pa s)	2.0×10^{-5}
Specific porous area of the catalyst layer, A_{v1} (mm^{-1})	8,000
Mean agglomerate diameter, D_{agg} (mm)	6.1E−3
Agglomerate characteristic length, L (mm)	1.02×10^{-3}
Agglomerate diffusion parameter, δ/a (mm^2)	2.42×10^{-3}
Diffusivity of oxygen in the polymer, D_{m,O_2} (mm/s)	1.15×10^{-4}
Diffusivity of hydrogen in the polymer, D_{m,H_2} (mm/s)	2.29×10^{-4}
Reference anode exchange current density, $i_{0,a}$ (A/mm^2)	5.0×10^{-6}
Reference cathode exchange current density, $i_{0,c}$ (A/mm^2)	6.0×10^{-10}
Anodic transfer coefficient, α_a	12
Cathodic transfer coefficient, α_c	3/2
Oxygen reference concentration, $c_{O_2,ref}$ (mol/mm^3)	4.55×10^{-9}
Hydrogen reference concentration, $c_{H_2,ref}$ (mol/mm^3)	2.17×10^{-8}
Convective mass transfer coefficient, h_{mass} (s^{-1})	100
Solubility coefficient for the cathode, $h_{d,c}$ (K^{-1})	4.09E−4
Solubility coefficient for the anode, $h_{d,a}$ (K^{-1})	1.82E−3
Open circuit voltage, V_{oc} (V)	1.0

numerical techniques [9,13]. The domain is divided into 35 × 147 elements. Mapped meshing was used to maintain a sufficient mesh density throughout the model domain. A sensitivity analysis was conducted by doubling the number of elements in the mesh. The solution changed on average by less than 0.33% and so was assumed to be mesh independent.

3. Results and discussion

Fig. 7 shows an experimental polarization data set for a 50 cm^2 ElectroChem cell operating at the conditions given in Table 6. Also plotted in Fig. 7 is a curve showing the cell polarization predicted using the model operating under the same conditions. The numerical results are consistent with the data set over the entire operating range.

In this model, the transport of reactants through the catalyst layer occurs along two parallel pathways. The first

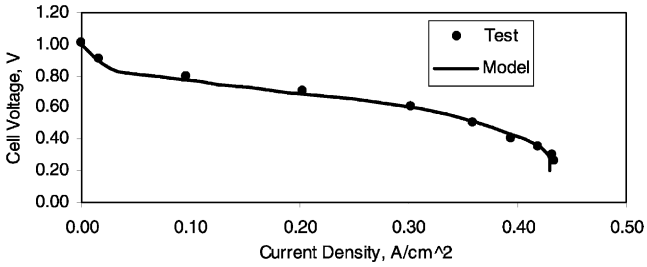

Fig. 7. Numerical and experimental performance curves for test cell.

Table 6
Physical conditions for fuel cell test

Test parameter	Value
Anode inlet pressure (psig)	24.9
Cathode inlet pressure (psig)	25.5
Cell temperature (K)	348
Anode volume flow rate (SLPM)	2.5
Cathode volume flow rate (SLPM)	50
Anode relative humidity (%)	65
Cathode relative humidity (%)	60

is gas transport by diffusion and advection through the macro-pores within the catalyst layer (shown in Fig. 2). As the reactants pass through the pores, they dissolve into the catalyst agglomerates and diffuse inward through the surrounding polymer to the carbon-supported platinum reaction sites. For a fixed volume of carbon-supported catalyst particles, a change in the catalyst layer void fraction requires a corresponding change in the fraction of ionomer in the catalyst layer. Fig. 8 shows cell performance as void fraction is changed at a cell voltage of 0.5 V.

The optimal catalyst layer void fraction for the test MEA at this voltage is 0.04 or 4%. The results in Fig. 8 show that for void fractions less than 0.04 the cell performance drops rapidly. This is due to rapidly increasing concentration overpotential. As the void fraction and permeability decrease, reactant transport by diffusion and advection within the catalyst layer drops sharply. The effect is exacerbated by the fact that the catalyst layers on the test MEA are relatively

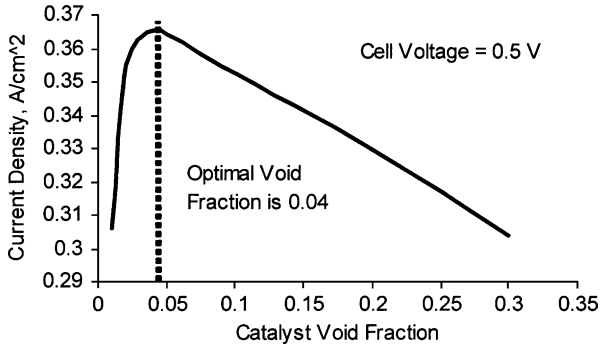

Fig. 8. Cell performance variation with catalyst layer void fraction.

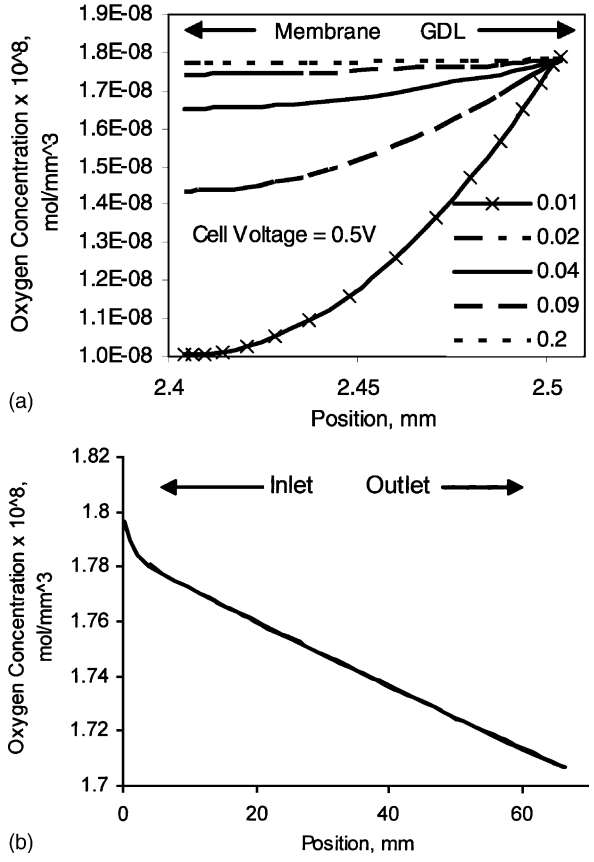

Fig. 9. (a) Oxygen concentration change across the cathode catalyst layer. (b) Oxygen concentration change down the cathode flow channel, 9% void fraction. Inlet conditions as per Table 4.

thick, 100 μm. Catalyst layer thickness also plays a role in the performance drop off for void fractions greater than 0.04. As the void fraction increases, the ionomer fraction must decrease. Thus, while an increase in porosity improves mass flow and reduces concentration overpotential, it also increases the ohmic overpotential. Since the catalyst layers are so thick (relatively long ionic conduction pathway), the test cell is particularly sensitive to changes in ionic conductivity.

Fig. 9a shows the variation of oxygen concentration through the fuel cell (perpendicular to the flow direction) as the void fraction is varied. Fig. 9b shows the oxygen variation down the channel at the catalyst layer/membrane interface.

Fig. 9a shows that the overall decrease in concentration of oxygen through the catalyst is not a linear function of void fraction. As the void fraction changes from 0.04 to 0.02, the concentration drop increases by roughly 15%. As the void fraction changes from 0.02 to 0.01 the concentration drop increases by approximately 44%. This can be attributed to the effect of permeability on reactant transport. Fig. 9b shows that at the base case conditions, the oxygen concentration drops by 5% down the channel. The non-linear portion of the curve can be attributed to developing flow effects and higher local reaction rates.

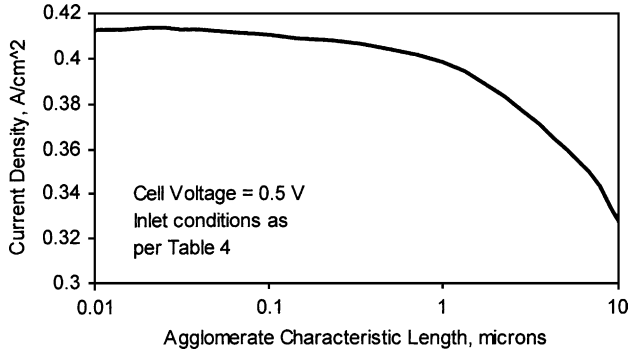

Fig. 10. Cell performance variation with characteristic length of the catalyst agglomerates.

Fig. 10 shows the effect of the characteristic length of the catalyst agglomerates on fuel cell performance.

The results in this figure indicate that the size of the catalyst agglomerates can significantly affect cell performance. As agglomerate size increases, the reactants must diffuse through a greater distance to reach the catalyst sites, thus causing an increase in concentration overpotential. The smallest possible characteristic length is about 0.01 μm, which is the ratio of the volume to surface area for a single catalyzed carbon support particle with an assumed spherical geometry (~50 nm diameter). One way to reduce the characteristic length is to create a catalyst layer with smaller agglomerates. Another way is to control the shape of the agglomerates, i.e. use a structure with a low volume to surface area ratio, such as a ribbon. For the test cell used in validating the model, the average characteristic agglomerate length was determined from the SEM analysis to be about 1 μm.

4. Conclusions

A steady state, two-dimensional model of a proton exchange membrane fuel cell has been developed for the purpose of predicting fuel cell behavior over a range of operating conditions and for use as a design tool. Work currently underway will expand this model to three-dimensional and incorporate liquid water transport.

Results from our two-dimensional model were presented and validated with experimental data. Electron microscopy was found to be an effective method for determining certain physical parameters used in the model such as catalyst void fraction, agglomerate size, and catalyst layer thickness. The void fraction of the catalyst layer was found to significantly influence cell performance. Model results show that a void fraction of 0.04 in the catalyst layer is optimal for the ElectroChem MEA on which the model is based. In addition increasing the agglomerate characteristic length leads to a decrease in cell performance primarily due to increased diffusive resistance to reactant flow. Control of catalyst layer structure at the microscopic level, particularly void fraction

and characteristic agglomerate length, could lead to better cell performance in the high current density region where concentration overpotential is most significant.

Acknowledgements

This work was performed at Virginia Polytechnic Institute and State University and funded in part with support received from the United States Department of Energy under Contract No. DE-FC36-01G01186. Additional funding was provided by the National Science Foundation and the DOE GATE program. The authors also acknowledge the support provided by Dr. Rita Schnipke of Blue Ridge Numerics Inc., for her help in implementing the model with CFDesign™.

References

[1] T.E. Springer, T.A. Zawodzinski, S. Gottesfeld, Polymer electrolyte fuel cell model, J. Electrochem. Soc. 138 (8) 2334–2341.
[2] D.M. Bernardi, M.W. Verbrugge, A mathematical model of the solid-polymer-electrolyte fuel cell, J. Electrochem. Soc. 139 (9) 2477–2490.
[3] K.A. Starz, J. Koehler, K. Ruth, M. Vogt, Advanced MEA Technology of Mobile PEMFC Applications, Fuel Cell Power for Transportation, SP-1691, 2002.
[4] K. Broka, P. Ekdunge, Modelling the PEM fuel cell cathode, J. Appl. Electrochem. 27 (1997) 281–289.
[5] B Olsommer, Mathematical Model for a PEM Fuel Cell, Internal Report, Energy Management Institute, Mechanical Engineering, Virginia Polytechnic and State University, Blacksburg, VA, 2000.
[6] B. Eaton, M.R. von Spakovsky, M.W. Ellis, D.J. Nelson, B. Olsommer, N. Siegel. One-dimensional, transient model of heat, mass, and charge transfer in a proton exchange membrane, in: Proceedings of International Mechanical Engineering Congress and Exposition, IMECE'2001, ASME, AES, vol. 40, New York, NY, November 2001.
[7] D. Genevey, M.R. von Spakovsky, M.W. Ellis, D.J. Nelson, B. Olsommer, F. Topin, N. Siegel, N. Montel, Transient Model of the Heat, Mass and Charge Transfer as well as Electrochemistry in the Catalyst Layer of a PEMFC, in: Proceedings of International Mechanical Engineering Congress and Exposition, IMECE'2002, ASME IMECE Paper No. 33322, New York, NY, November 2002.
[8] T. Zhou, H. Liu, 3-D model of proton exchange membrane fuel cells, in: Proceeding of the ASME Heat Transfer Division, HTD, vol. 366–361, 2000.
[9] V. Gurau, H. Liu, S. Kakac, Two-dimensional model for proton exchange membrane fuel cells, J. AIChE 44, 2410–2422.
[10] S. Um, C.Y. Wang, K.S. Chen, Computational fluid dynamics modeling of proton exchange membrane fuel cells, J. Electrochem. Soc. 147 (12) (2000) 4485–4493.
[11] S. Shimpalee, S. Dutta, J.W. Van Zee, Numerical prediction of local temperature and current density in a PEM fuel cell, in: Proceedings of the ASME Heat Transfer Division, HTD, vol. 366–361, 2000.
[12] D. Natarajan, T.V. Nguyen, A two-dimensional, two-phase, multi-component, transient model for the cathode of a proton exchange membrane fuel cell using conventional gas distributors, J. Electrochem. Soc. 148 (12) 1324–1335.
[13] S. Patankar, Numerical Heat Transfer and Fluid Flow, Hemisphere, Washington, DC, 1980.